Nanotechnology

PAPER • OPEN ACCESS

Fate assessment of commercial 2D MoS_2 aqueous dispersions at physicochemical and toxicological level

To cite this article: Brixhilda Domi *et al* 2020 *Nanotechnology* **31** 445101

OPEN ACCESS
IOP Publishing
Nanotechnology

Nanotechnology **31** (2020) 445101 (13pp)
https://doi.org/10.1088/1361-6528/aba6b3

Fate assessment of commercial 2D MoS_2 aqueous dispersions at physicochemical and toxicological level

Brixhilda Domi[1], Kapil Bhorkar[2,3], Carlos Rumbo[1], Labrini Sygellou[2], Spyros N Yannopoulos[2], Roberto Quesada[4] and Juan Antonio Tamayo-Ramos[1]

[1] International Research Centre in Critical Raw Materials-ICCRAM, Universidad de Burgos, Plaza Misael Banuelos s/n, 09001 Burgos, Spain
[2] Foundation for Research and Technology Hellas – Institute of Chemical Engineering Sciences (FORTH/ICE-HT), P.O. Box 1414, GR-26504 Rio-Patras, Greece
[3] Univ Rennes, CNRS, ISCR - UMR 6226, F-35000 Rennes, France
[4] Departamento de Química, Facultad de Ciencias, Universidad de Burgos, 09001 Burgos, Spain

E-mail: ja.tamayoramos@gmail.com

Received 5 June 2020, revised 5 July 2020
Accepted for publication 16 July 2020
Published 7 August 2020

Abstract

The physicochemical properties and the toxicological potential of commercially available MoS_2 nanoparticles with different lateral size and degradation stage were studied in the present research work. To achieve this, the structure and stoichiometry of fresh and old aqueous suspensions of micro-MoS_2 and nano-MoS_2 was analyzed by Raman, while x-ray photoelectron spectroscopy allowed to identify more quantitatively the nature of the formed oxidized species. A, the toxicological impact of the nanomaterials under analysis was studied using adenocarcinomic human alveolar basal epithelial cells (A549 cells) and the unicellular fungus *S. cerevisiae* as biological models. Cell viability assays and reactive oxygen species (ROS) determinations demonstrated different toxicity levels depending on the cellular model used and in function of the degradation state of the selected commercial nanoproducts. Both MoS_2 nanoparticle types induced sublethal damage on the A549 cells though the increase of intracellular ROS levels, while comparable concentrations reduced the viability of yeast cells. In addition, the old MoS_2 nanoparticles suspensions exhibited a higher toxicity for both human and yeast cells than the fresh ones. Our findings demonstrate that the fate assessment of nanomaterials is a critical aspect to increase the understanding on their characteristics and on their potential impact on biological systems along their life cycle.

Keywords: molybdenum disulfide, nanoparticles, fate, physicochemical composition, toxicity, oxidative stress, cell viability

(Some figures may appear in colour only in the online journal)

1. Introduction

Two-dimensional (2D) layered materials include a wide range of compounds such as graphene-based nanomaterials, transition metal dichalcogenides (TMDs), hexagonal boron nitride (h-BN), layered metal oxides and other compounds [1]. Due to their atomic or nanoscale thickness and large lateral size [2], 2D layered materials are suitable for biological and biomedical applications such as drug delivery, tissue engineering, bioimaging and biosensing [3]. Layered TMD nanomaterials such as molybdenum disulfide (MoS_2) represent an emerging class of 2D materials [4]. The bulk crystal is organized by covalently bonded monolayers stacked vertically with

weak van der Waals forces, which enable the possibility to easily exfoliate it into monolayer nanosheets, like graphite and h-BN. One of the main industrial application of layered MoS_2 is solid lubrication, and the potential of 2D MoS_2 films as solid lubricants for micro- and nanoscale mechanical systems is being explored too [5]. The large surface area of the layered nanosheets facilitates their biological interaction with cell membranes [6], and the distinctive physicochemical characteristics of MoS_2 have attracted considerable interest for the development of functional nano-agents for biosensing [7], drug delivery [8], cancer therapy [9], in conjunction with other biomedical applications such as tissue regeneration [10] and antibacterial effects [11]. However, it has been reported that MoS_2 nanomaterials can induce cell membrane damage in different unicellular systems [12].

Given the above context, assessing the toxicity of MoS_2 biological systems is an essential matter. Specific parameters such as lateral dimensions, number of layers, surface area, purity, shape, and size can substantially influence the interaction between MoS_2 and biological systems [1]. For that reason, the same compound can show different antibacterial and cytotoxic mechanisms depending on different physicochemical parameters. Overall, understanding how MoS_2 nanoparticles interact with cellular models and their components is important to identify their safety and biocompatibility. However, while a great progress has been achieved in understanding how safe are 2D nanosheets such as graphene and its derivatives, there is still limited knowledge about the toxicological potential of others derived from different layered materials, like those from the TMD family. Recently, toxicological studies of 2D MoS_2 have been undertaken, with particular attention to mammalian cell lines. For instance, the interaction between MoS_2 and human cell lines has been studied using tumoral cells, such as adenocarcinomic human alveolar basal epithelial cells A549, gastric adenocarcinoma epithelial cells AGS and breast cancer epithelial cells MCF, and normal like epithelial kidney cells HEK293f and keratinocytes cells HaCaT cell lines [13–16]. The aim of these studies was to investigate different parameters such as cytotoxicity, cellular uptake and inflammatory responses using several cell lines that could represent the human potential exposure routes. Others have investigated the interaction between 2D MoS_2 with microbial systems, such as Gram-positive and Gram-negative bacteria, to determine the potential antibacterial activity of the nanomaterial and to identify potential toxicity pathways [17]. The availability of studies analyzing the toxicological effect of MoS_2 flakes on fungal species is even more scarce. To date, only two studies using bulk MoS_2 and chitosan functionalized MoS_2 (CS-MoS_2) nanosheets have investigated the toxicological properties of the TMDs using the yeast *S. cerevisiae* as a fungal model [18, 19]. Therefore, to obtain a more comprehensive understanding on the toxicological potential of 2D MoS_2 additional studies are needed with their focus put on physicochemical aspects and fate of the nanomaterial, paying attention to additional biological models and biomolecules to those already assessed. While the availability of research works comparing the toxicity of pristine and transformed nanoproducts is very low, assessing the stability and degradation of TMDs is an essential aspect to increase the understanding on the impact of these materials and their transformation products in biological systems. MoS_2 nanosheets have been shown to be thermodynamically and kinetically unstable to oxidation under ambient conditions in aqueous media, resulting in measurable morphological changes and in the release of soluble molybdenum and sulfur species, generating protons able to destabilize the remaining sheets [20, 21].

In the present study, we investigate the biological effects of commercially available mono- and bilayer MoS_2 flakes of different lateral sizes with distinct integrity stages, using different cell models, such as adenocarcinomic human alveolar basal epithelial cells (A549) [22] and the yeast *S. cerevisiae* [23]. Raman spectroscopy and x-ray photoelectron spectroscopy (XPS) were used to determine the extent of oxidation and to identify the relevant species derived from MoS_2 nanosheets in water suspensions. Hence, we analyzed to what extent the nanomaterials oxidation influence the toxicological responses of the laboratory models used. The obtained results provide information about the time-dependent oxidation degree of MoS_2 nanoparticles, which is critical to understand and regulate issues related to their environmental fate, and their impact on different biological models.

2. Materials and methods

2.1. Materials and reagents

Most chemicals and reagents were purchased from Sigma-Aldrich (Merck KGaA, Darmstadt, Germany) and Acros Organics (Thermo Fisher Scientific Inc., Madrid, Spain). Monolayer molybdenum disulfide (micro-MoS_2) and nano size monolayer molybdenum disulfide (nano-MoS_2) were purchased at ACS material®. The 10 months old (old) water suspensions were obtained by storing purchased bottles for 10 months at 4 °C.

2.2. AFM and TEM

For AFM analysis, samples were dropped on a mica surface from aqueous solutions by drop-casting. Images were recorded in AC mode (tapping mode) with a CYPHER ES instrument from Asylum Research (Oxford Instruments), using silicon cantilevers AC160TS-R3 with aluminum reflex coating (Olympus) and tip radius <10 nm. The analysis was completed using a set point of 500, 72 mV, a drive amplitude of 791.16 and a drive frequency of 268.639. IGOR Pro 6.2 (Asylum Research) was used for data acquisition and control. ARgyle software was utilized for all the images analysis. For TEM analysis samples were placed on Lacey Carbon Type-A, 300 mesh, copper grids, and visualized and photographed using a JEOL JEM-1011HR TEM coupled with a Gatan Erlangshen ES1000W camera at the Microscopy Unit from the University of Valladolid.

2.3. Raman analysis

Raman spectra were recorded at ambient conditions from the same drop-casted samples using the 441.6 nm radiation as an excitation source emerging from a He-Cd laser (Kimon). The laser light was focused by a 50× objective creating a focusing area of 1–2 μm. The scattered light was collected by the same objective and analyzed using by the LabRam HR800 (Jobin-Yvon) spectrometer operating at a spectral resolution of $\sim$2.0 cm^{-1}. A very low light fluence (275 μW) on the maple was used to avoid heat induced effects (oxidation and decomposition). The Raman mode of Si single crystal at 520 cm^{-1} was used to calibrate the wavenumber scale of the spectra.

2.4. XPS

The surface analysis study was performed in a UHV chamber (P < 10^{-9} mbar) equipped with a SPECS LHS-10 hemispherical electron analyzer and a dual anode x-ray gun. The XPS measurements were carried out at room temperature using the unmonochromatized AlK*a* radiation under conditions optimized for maximum signal (constant ΔE mode with pass energy of 97 eV giving a full width at half maximum, FWHM, of 1.7 eV for the $Ag3d_{5/2}$ peak). The XPS core level spectra were analyzed using a fitting routine, which allows the decomposition of each spectrum into individual mixed Gaussian-Lorentzian components after a Shirley background subtraction. The samples were prepared by drop-casting aliquots of the MoS_2 water dispersions onto 1 × 1 cm^2 Si wafers. Errors in the quantitative data are in the range of $\sim$10% (peak areas), while the accuracy for binding energy (BEs) assignments is $\sim$0.1 eV.

2.5. A549 cell culture

The human alveolar carcinoma epithelial cell line A549 (ATCC, CCL-185) was utilized for toxicological evaluation. Cells were grown in DMEM medium (Dulbecco's Modified Eagle Medium) supplemented with 10% fetal calf serum (FCS), 1% penicillin, 1% streptomycin and grown in a humidified incubator at 37 °C (5% CO_2). In all assays performed, cells were trypsinized after 24 h of incubation, at 90% confluency. Around 3 × 10^4 cells (suspended in 200 μl of growth media) in each well of a 96 well micro-plate were allowed to adhere and grow for 24 h.

2.6. Dispersions of micro and nano MoS_2 for A549 cells toxicity assays

The solutions for the Neutral Red assay were prepared using the commercial stocks (1 g l^{-1}) in treatment medium (DMEM 1% FCS) and sterile water to prepare final stocks of 160 mg l^{-1}. Afterwards, to prepare the solutions for the reactive oxygen species (ROS) assay, the commercial stocks were diluted in HBSS (Hank's Balanced Salt Solution) 10× and sterile water. After an initial sonication of the mother stock samples, the suspended (micro- and nanoscale) MoS_2 samples were vortexed for few seconds to homogenize the final solution for the toxicity assays.

2.7. A549 cells Neutral Red assay

After 24 h incubation, cell culture medium was discarded and cells were washed DPBS (Dulbecco's phosphate-buffered saline). The central wells of the 96 well micro-plate were incubated with treatment medium with the final concentration of 20, 40, 80 and 160 mg l^{-1}. Cells were then incubated for 24 h at 37 °C, under 5% CO_2. Successively to the 24 h exposure to the nanomaterials, cells were washed and incubated with 100 μl of the Neutral Red solution for 2.5 h at 37 °C in the dark. The Neutral Red solution was prepared as follows: 1:100 dilution of the Neutral Red stock (3-amino-7-dimethylamino-2-methyl-phenazine hydrochloride) was prepared in treatment medium (DMEM 1% FCS), previously incubated for 24 h at 37 °C and centrifuged at 3000 rpm for 10 min to precipitate crystals formations. After incubation, Neutral Red Solution and nanoparticles were discarded and each well washed with DPBS. Afterwards, 100 μl of a fixation solution (formaldehyde 4%) was added to each well for 2 min, and cells were washed again. Each well was treated with 150 μl of solubilization solution (50% ethanol 96%, 49% H_2O, 1% acetic acid) at room temperature for 10 min with shaking and covered from light. To measure the fluorescence, 100 μl of each extract from cells was transferred into a black opaque 96 micro-well plate. The micro-plate reader spectrophotometer (Synergy-HT, BioTek) was used to read fluorescence at excitation 525/30 nm and emission at 640/645 nm.

2.8. A549 cells ROS assay

The quantitative measurement of intracellular ROS was investigated using 2,7-dichlorofluorescin diacetate (DCFH-DA). The DCFH-DA inactively pass the cell's membrane and reacts with the intracellularly ROS. The last product of this reaction is the highly fluorescent compound dichlorofluorescein (DCF). Twenty-four hours after seeding, A549 cells were transferred in a 96 micro-well plate, washed twice with HBSS and incubated with 200 μl of DCFH-DA (50 M) for 30 min at 37 °C. After the exposure time, cells were washed with HBSS and incubated with 200 μl of nanoparticles solutions at 20, 40, 80 and 160 mg l^{-1}. The ROS production is measurable due to the oxidation reaction of DCFH to dichlorofluorescein (DCF) intracellularly. Fluorescence intensity was measured after 1 h incubation, at 485 nm excitation and 520 nm emission using a microplate reader (Synergy-HT, BioTek). The experiment was repeated three times.

2.9. Yeast culture

S. cerevisiae B4741 was maintained in liquid and agar media of YPD medium (1% yeast extract, 1% yeast bacto-peptone, 2% glucose). In exposure experiments, cells were firstly grown on a rotary shaker at 185 rpm at 30 °C until the final OD_{600} nm was equal to 1 (exponential phase).

2.10. Yeast colony forming units (CFUs) determination

A 24 multi-well plate was used for the incubation of yeast (OD_{600} nm = 1) in the presence of micro-MoS_2 and

nano-MoS_2. The concentration ranges tested for all the samples were 160 and 800 mg l^{-1}, for 2 and 24 h. To define cells viability after each exposure time, aliquots were diluted 10^4 times, in case of 2 h exposure, and 10^5 times, in case of 24 h exposure, and 100 μl of the diluted suspensions was plated on solid YPD medium (6% agar). Plates were incubated at 30 °C for 48 h and CFUs were determined.

2.11. Yeast ROS assay

For the evaluation of ROS, a 24 multi well plate was used. Cells with a final OD_{600} nm equal to 1 (exponential phase) were centrifuged (for 3 min at 4000 rpm), washed and suspended in 12.5 ml of DPBS (OD_{600} nm = 16). Successively, the commercial stock with dry CM-H2DCFDA (General Oxidative Stress Indicator) was suspended in 20 μl of DMSO (dimethyl sulfoxide) and the final concentration of the reagent is equal to 4.33 mM. Subsequently, cells were incubated with 20 μl of CM-H2DCFDA in the dark for 60 min at 30 °C and 185 rpm. Cells were then centrifuged, washed with DPBS and suspended in 5 ml YPD 5× liquid medium. Then, cells were incubated with the nanomaterial suspensions (final volume 1 ml) for 2 h at 30 °C and 185 rpm in the orbital shaker. The concentrations tested were 160 and 800 mg l^{-1}. After the 2 h incubation, 500 μl of each sample were centrifuged and washed two times with DPBS. Next, each sample was suspended in 200 μl of AcLi (lithium acetate) 2 M and incubated for 2 min with moderate agitation in the thermomixer at 400 rpm. Thus, cells were centrifuged and the pellet was suspended in 200 μl OF 0.01% SDS (sodium dodecyl sulfate) + chloroform (150 μl in 40 ml) and incubated for 2 min. Afterwards, 150 μl of each sample was transferred on a black opaque 96 microwell plate and the fluorescence was measured at 485 nm excitation and 528 nm emission using a microplate reader (Synergy-HT, BioTek).

2.12. Statistics

Statistical analysis data are presented as mean ± SD. Differences between the negative control and the treatment with MoS_2 samples were established using a Student's *t*-test. The one-way analysis of variance (ANOVA) was used for multiple comparisons, followed by Dunnet's post hoc test. Statistical tests were carried out using Prism 6.0 (GraphPad Prism, GraphPad Software, Inc.). Statistical significance is considered with a *P* values of less than 0.05. Each experiment was repeated three times in triplicate.

3. Results and discussion

3.1. Selection and characterization of commercial molybdenum disulfide

In the present work, commercial water suspensions (1 mg ml^{-1}) and powders of MoS_2 platelets prepared using lithium-based intercalation method and supplied by ACS material® were selected: monolayer molybdenum disulfide (micro-MoS_2) and nano size monolayer molybdenum disulfide (nano-MoS_2). The characterization information provided by the supplier indicates a lateral size of 0.2–5 μm and a thickness of 1 nm for the micro-MoS_2 powder, and a diameter of 20–500 nm and the thickness of 1 nm for the nano-MoS_2 material. To further understand the morphologic features of both MoS_2 samples, AFM (figure 1) and TEM (figure 2) analyses were performed by drop-casting the samples on a mica surface and carbon-coated copper grids, respectively. Even if drop-casting and drying nanoparticle monodispersions can induce aggregated forms, for instance, due to surface dewetting, preventing the accurate visualization and quantification of particle size distribution, the combination of AFM and TEM allowed to observe a population of both nanoparticle types as well as morphological features. As can be seen in figure 1, AFM images of the two MoS_2 products showed the presence of possible aggregates with different shape and a significant population of particles with a lateral size distribution in the nanoscale range, with a round shape. Height profile curves displayed gave insights into the thickness of the observed nanoforms. TEM images confirmed that the both the micro- and nano-MoS_2 particles have a 2D platelet-like shape as previously described for this type of nanomaterials (figure 2) [24]. No clear differences amongst both products could be observed in terms of size, aggregation state or morphological characteristics.

To explore the structure and stoichiometry of micro- and nano-MoS_2 samples at different integrity states, Raman spectra of recently purchased (fresh) and 10 months old (old) water suspensions were collected and analyzed. Since the probed area (1–2 μm in diameter) is quite small to provide reliable information with a single measurement, various points of drop-casted films on Si were analyzed. The measurements showed a very homogeneous behavior of the spectra at various points. Representative Raman spectra of the fresh and old micro- and nano-MoS_2 suspensions are shown in figure 3. The first order Raman spectrum of MoS_2 is characterized by peaks with symmetries A_{1g} and E^1_{2g}. These peaks are observed in all the spectra displayed, at near 405 cm^{-1} and 385 cm^{-1}, respectively. A strong band near 520 cm^{-1} in all spectra originates from the Si substrate. The Raman spectra of the pristine (dry) powders are also presented, revealing that the particles are free of oxides or other contaminants. The samples stored in water present considerable changes in Raman spectra, since the fraction of MoS_2 decreases systematically due to oxidation. The difference in the A_{1g} and E^1_{2g} modes amounts to $\Delta\omega \approx 22.8$ cm^{-1} and ≈ 23.0 cm^{-1} for the nano- and micro-sized MoS_2, respectively. These values indicate a thickness of the particles of about 2–3 monolayers [25]. For better visualization, the spectra of nano-MoS_2 was enhanced by factors of 2 and 10 for the fresh and old samples, respectively. The Raman data indicates that nano-MoS_2 is more vulnerable to oxidation during water storage, in comparison to micro-MoS_2. The frequency difference of the A_{1g} and E^1_{2g} Raman bands becomes smaller in soaked samples, as $\Delta\omega \approx$ 20–21 cm^{-1} indicates the prevalence of flakes with mono- or bi-layer thickness for both the micro- and nano-MoS_2 samples. For comparison, the

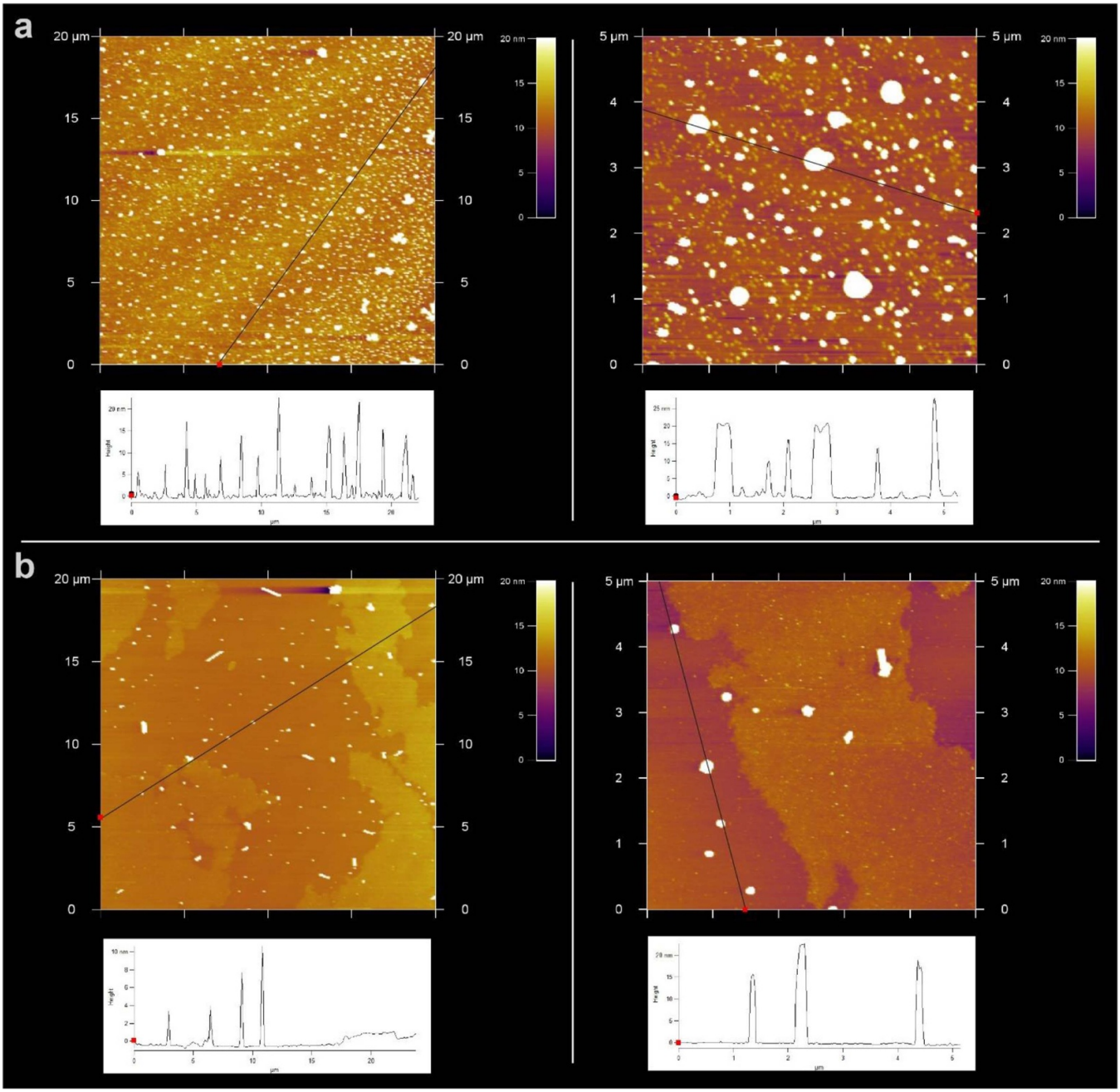

Figure 1. AFM images and corresponding height profiles of micro-MoS_2 (a) and nano-MoS_2 (b). Molybdenum disulfide dispersions with a concentration of 20 mg l^{-1} were deposited by drop-casting on a mica surface.

spectrum of the MoO_3 crystal is also shown in figure 3. The most intense Raman band of MoO_3 is located at 820 cm^{-1}, while a weak broad band appears near this energy in the spectra of the oxidized samples. Additional Raman bands appear in the spectra of the oxidized samples at ∼150 and ∼219 cm^{-1}. Raman spectra of oxides [26] show the existence of bands near these wavenumbers which correspond to MoO_x species ($2 < x < 3$). A broader composite band with components at ∼458 and ∼472 cm^{-1} appears for particles dispersed in water. This band is strongly enhanced in case of resonance Raman scattering of MoS_2, typically recorded with 632.8 nm near bandgap excitation (∼1.96 eV). The appearance of this band in the current spectra and its intensification upon increasing the soaking time indicates the continuous change of the particle composition. The particle structure changes gradually by oxidation; this causes bandgap widening, as the oxidized species come into resonance with the excitation source. The creation of mixed oxysulfide MoS_xO_y species could in principle be responsible for this effect.

In addition to Raman, XPS was employed to identify more quantitatively the nature of the oxidized species. The same samples used for Raman scattering were studied by XPS. This technique probes a much larger area (∼0.5 mm^2) in comparison to Raman scattering, hence providing a consistent

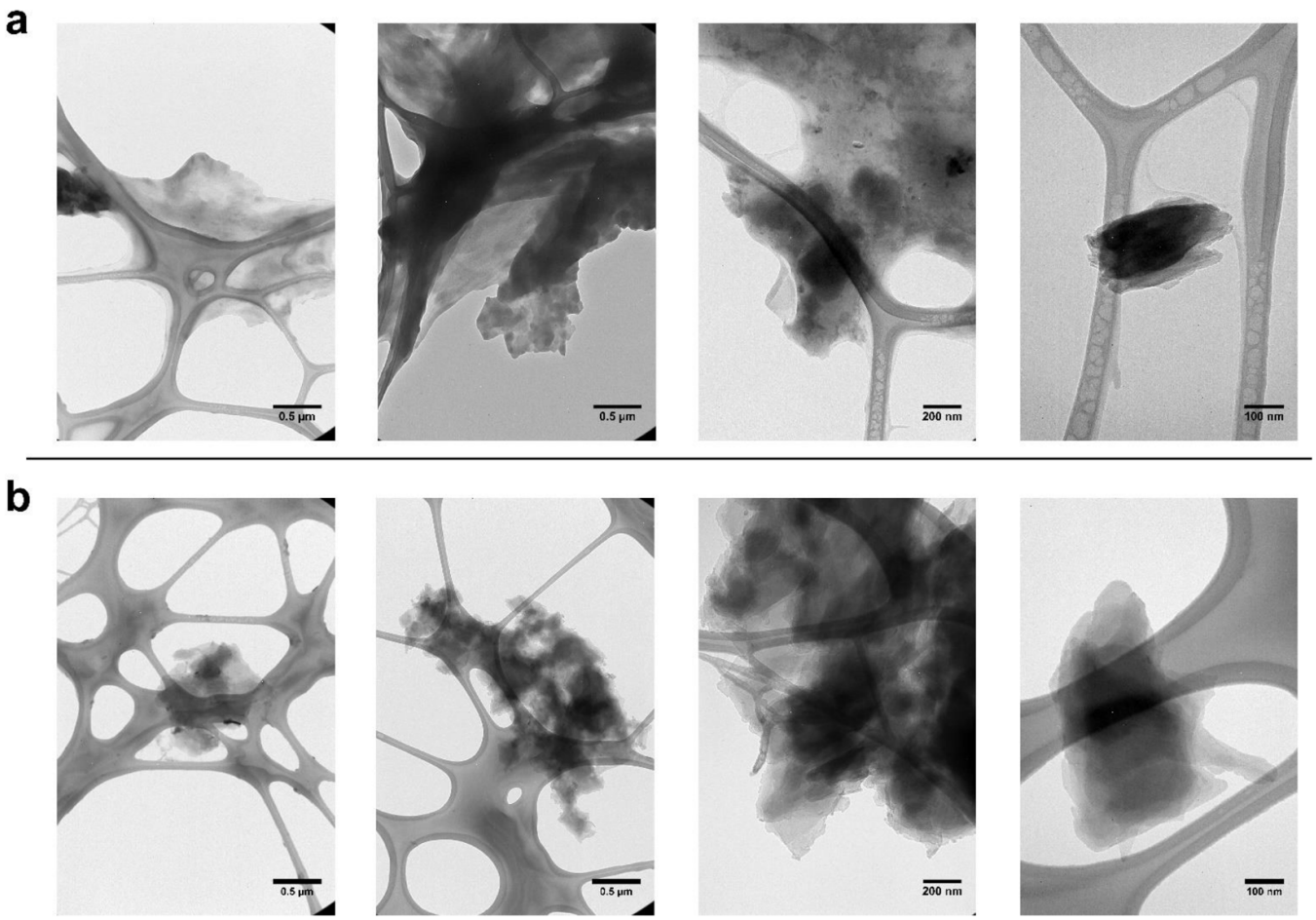

Figure 2. TEM images of micro-MoS_2 (a) and nano-MoS_2 (b). Molybdenum disulfide dispersions with a concentration of 20 mg l^{-1} were deposited by drop-casting on carbon-coated copper grids.

picture of the whole sample area. Figure 4 displays detailed XPS scans for the Mo3d peaks, in the samples under study. The Mo3d peak is deconvoluted into two doublets with a spin orbit splitting of 3.3 eV. The BE of $Mo3d_{5/2}$ at 233.1 ± 0.1 eV is assigned to MoO_3 [27] while that at 229.0 ± 0.1 eV has been associated to MoS_2 [28]. In the same energy region, the S2s band is present. This band consists of two components assigned to 2H-MoS_2 and to bonds of sulfur oxide. The obtained results show a progressive oxidation of the MoS_2 platelets in the water dispersion as a function of time, being more accelerated in the nano-MoS_2 sample.

To gain insight into the nature of the MoS_2 nanosheets oxidation process, the obtained S2p bands were analyzed into their components. Figure 5 displays representative XPS scans for the S2p peaks for the micro- and nanosized MoS_2 old samples. The S2p band is deconvoluted into four doublets with spin orbit splitting 1.2 eV. The BEs of the $S2p_{3/2}$ peaks and their assignment is as follows: (1) 162.0 ± 0.1 eV; S atom at the basal plane of MoS_2; (2) 163.5 ± 0.1 eV; unsaturated sulfur atoms; (3) 167.2 ± 0.1 eV; sulfates; (4) 168.4 ± 0.1 eV, thionates, $[S_n(SO_3)_2]^{2-}$ [28, 29], and or sulfonyl groups (-SO2-groups) [30].

3.2. Toxicology assessment using adenocarcinoma A549 human cells

The biological response towards the selected commercial MoS_2 nanoparticles (recently purchased (fresh) and 10 months old (old) water suspensions) was firstly assessed using the human lung (carcinoma) cell line A549, which represents alveolar type II cells, a potential target of nanomaterials after inhalation [31]. The cells were exposed to different concentrations of fresh and old micro- and nano-MoS_2 suspensions, up to 160 mg l^{-1}, for a period of 24 h. The Neutral Red assay was chosen to determine the cells viability in the described exposure conditions, as it is one of the most used cytotoxicity tests, including those that evaluate nanomaterials toxicity [32]. The method is based on the capability of viable cells to incorporate and bind the supravital dye Neutral Red inside the lysosomes, being amongst the most sensitive cytotoxicity tests [33]. As displayed in figure 6, cells exposed to both types of fresh and old MoS_2 nanosheets (160 mg l^{-1}) showed to have the same viability as the negative control. The same result was observed for the lower concentrations tested of the different nanoparticles suspensions, indicating that the viab-

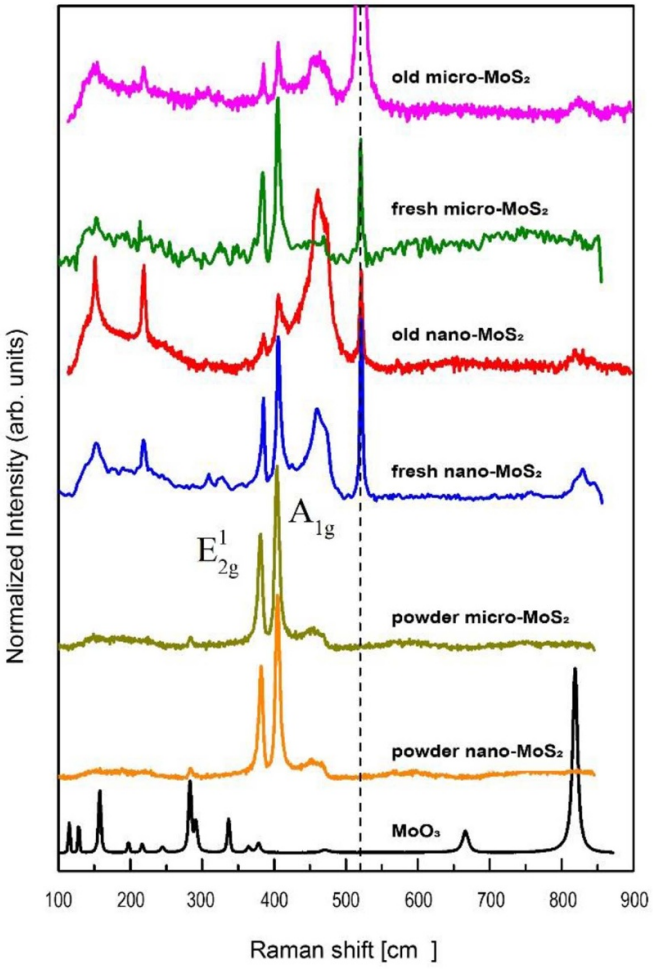

Figure 3. Raman spectra of the micro- and nanosized MoS_2 soaked in water (fresh and 10 months old). The spectra of the dry powders and the spectrum of MoO_3 are also shown for comparison.

ility of A549 cells is not negatively affected in the presence of micro-MoS_2 and nano-MoS_2, nor by their transformation and degradation products, at the studied conditions. In addition, no significant viability differences were observed between cells exposed to micro- and nano-MoS_2 particles.

The observed results are comparable to those reported for MoS_2 nanosheets obtained using methyllithium (Me-Li) as intercalating agent [12], where similar concentrations showed to elicit low cytotoxicity on A549 cells as well. In contrast, MoS_2 exfoliated with other intercalating reagents, such as n-butyllithium (n-Bu-Li) and tert-butyllithium (t-Bu-Li), had a stronger cytotoxic impact in the cells at the same concentration range. The potential toxicological effects of MoS_2 nanosheets against other human *in vitro* models has been investigated, like the cancer cell line TPH1 and the non-tumorigenic lung epithelial cell BEAS 2B, where no cytotoxicity was observed at concentrations up to 50 mg l^{-1} [34]. Interestingly, aggregated MoS_2 showed higher toxicological potential than that caused by 2D-MoS_2. More recent literature also reports the impact of MoS_2 nanoparticles present in aqueous dispersions and coatings, against other human cell line types [15].

Although no previous reports compare the potential toxicity of commercial pristine MoS_2 nanosheets with that of their transformation products, a recent study revealed the potential toxicity of two polyvinylpyrrolidone-modified 2H-phase MoS2 nanosheets oxidation products, such as MoO_3 and MoO_4^{2-}, in exposed HUVECs and SMMC-7721 cells [35]. The nanomaterial oxidation products showed ability to reduce the cell vitality in concentrations higher than 200 mg ml^{-1}. Interestingly, a study comparing the toxicity elicited by exfoliated TMDs and graphene derivatives, also indicated that MoS_2 toxicity up 200 mg l^{-1} is low, being lower as well than that induced by graphene oxide and derivatives [36].

Nanomaterials present at sublethal concentrations can still alter cell viability by inducing high levels of ROS [37], which frequently trigger programmed cell death (apoptosis) [38]. Hence, to obtain additional insights on the potential adverse biological effects of MoS_2 nanosheets on human cells we further investigated the oxidative stress levels of A549 cells exposed to the selected nanoparticles suspensions (fresh micro-MoS_2 and nano-MoS_2) and to their transformation products (old micro-MoS_2 and nano-MoS_2), using the DCFH-DA assay [39]. As done previously in the viability assay, the ROS generation was determined after 1 h exposure to concentrations up to 160 mg l^{-1} of fresh and old micro- and nano-MoS_2. In these conditions, no significant increase of oxidative stress levels were observed in exposed A549 cells. Recent studies investigating the possible cytotoxic effect of dispersible MoS_2 nanosheets on human dermal fibroblasts and hepatoma cells have reported increased oxidative stress in exposed cells. MoS_2 induced a dosage-dependent ROS production in human dermal fibroblasts, which showed an increase of ∼50% and ∼75% of ROS levels with respect to the control condition in cells exposed 100 and 200 mg l^{-1}, respectively [40]. The ROS induction by MoS_2 nanosheets on human hepatoma cells HepG2 was even more striking, with significantly higher oxidative stress levels being observed even in the presence of 2 mg l^{-1} [41].

In relation to the ROS levels observed in A549 cells exposed to the old nanoparticles suspensions, higher levels of oxidative stress were observed (figure 7(b)). Cells exposed to old micro- and nano-MoS_2 showed 3.6 and 3.1 times higher ROS levels, respectively, than the non-exposed cells. The significant oxidative levels induced by the old samples suggest a mixture toxicity effect derived from the MoS_2 nanosheets transformation products. For instance, MoO_3 is considered an irritant product, with reported animal carcinogenicity [42]. MoO_3 nanoplatelets were shown to induce ROS in iMCF-7 cells because of elevated ROS levels [43], but limited information is available on the toxicity of MoO_3 and other MoS_2 transformation products, such as molybdenum oxysulfide (MoO_xS_y) on different human cell lines.

3.3. Toxicology assessment using S. cerevisiae

The toxicity of MoS_2 nanosheets has been mostly studied in distinct human cell lines, while the impact of these nanomaterials and other 2D TMDs in other unicellular organisms is less known.

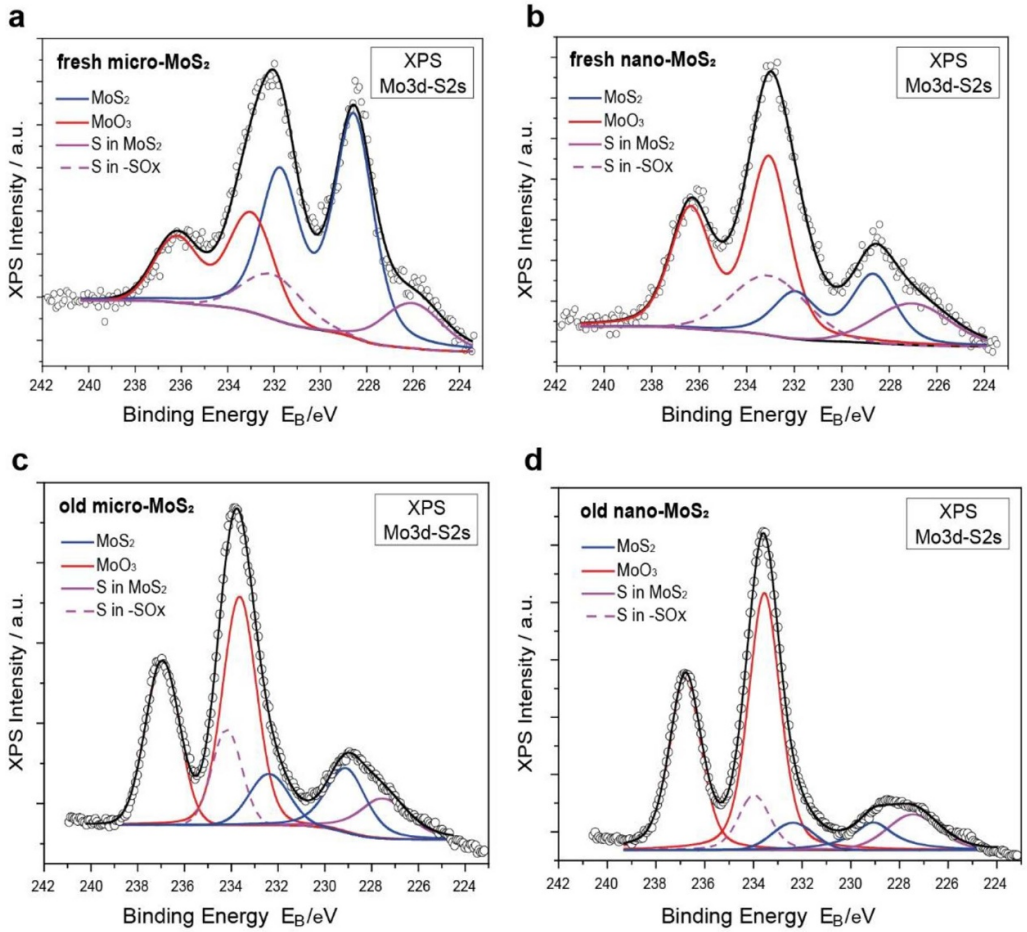

Figure 4. Deconvoluted Mo3d XP spectra of (a) fresh micro-MoS_2, (b) fresh nano-MoS_2, (c) old micro-MoS_2, and (d) old nano-MoS_2.

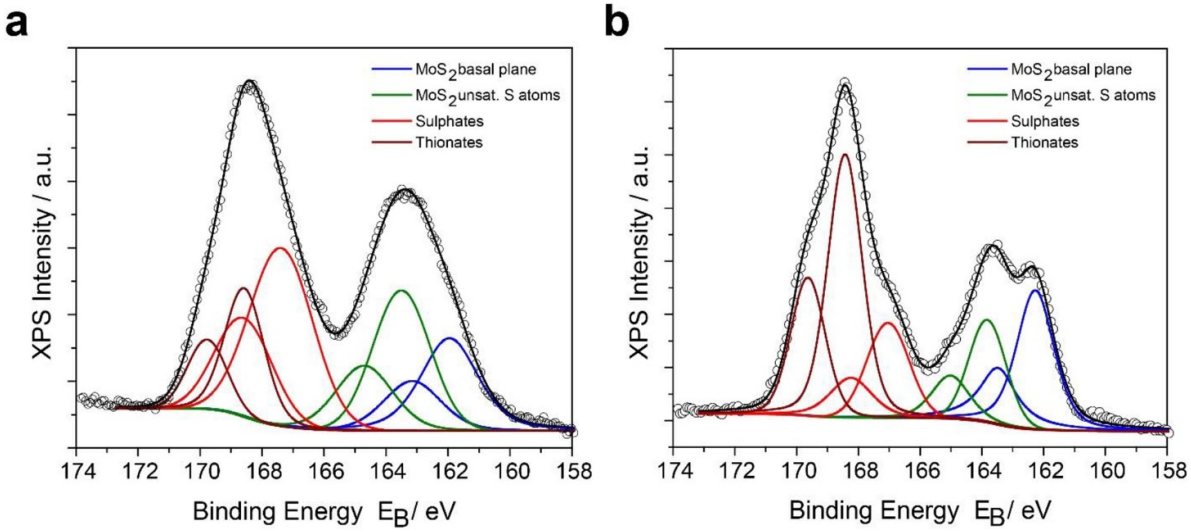

Figure 5. Deconvoluted S2p XP spectra of micro-MoS_2 (a) and nano-MoS_2 (b) samples obtained from old water suspensions.

For instance, in case of *S. cerevisiae*, another eukaryotic model commonly used in toxicology studies, only few reports have described the effect of MoS_2 forms on yeast cells, such as bulk MoS_2 and chitosan functionalized MoS_2 [18, 19]. Here, as previously described for the A549 cells, the impact of different concentrations of fresh and old MoS_2 nanosheets suspensions on the yeast strain BY4741 was analyzed. A CFUs determination of *S. cerevisiae* cells exposed to 160 and 800 mg l^{-1} of the different MoS_2 nanoforms for 2 and 24 h was performed (see Materials and methods) [44]. As displayed

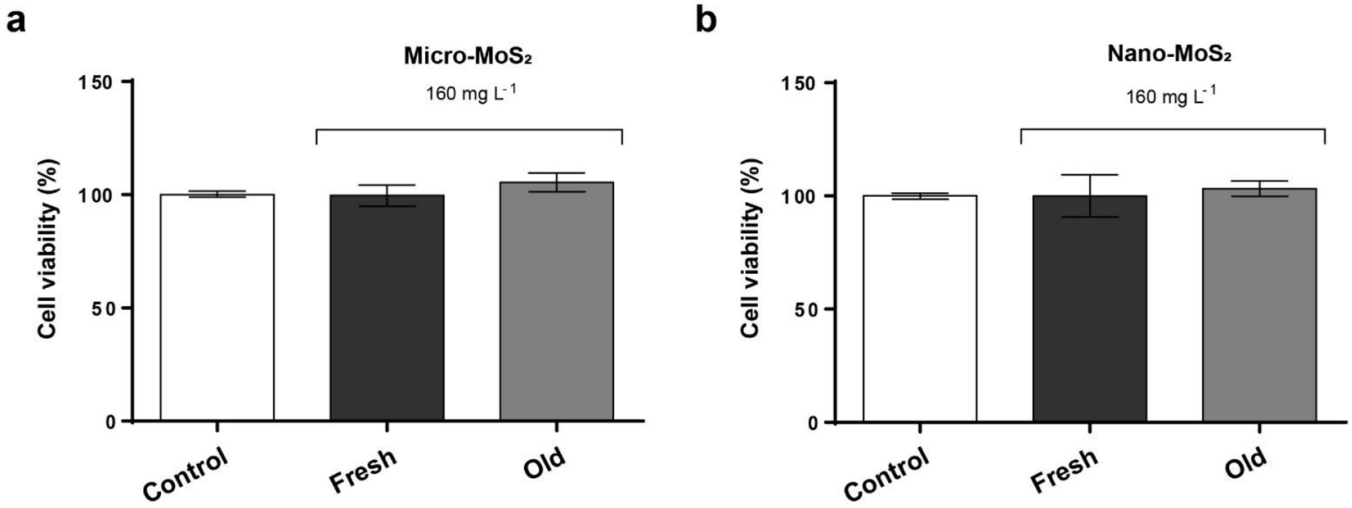

Figure 6. Viability of A549 cells (Neutral Red assay) exposed to 160 mg l^{-1} of fresh and old micro-MoS_2 (a) and nano-MoS_2 (b) for 24 h. Results are expressed as % of control (non-exposed cells). Data represent the mean (±standard deviation, SD) of three independent replicates. Differences were established using a one-way ANOVA followed by Dunnett's post hoc test to compare every mean with the control.

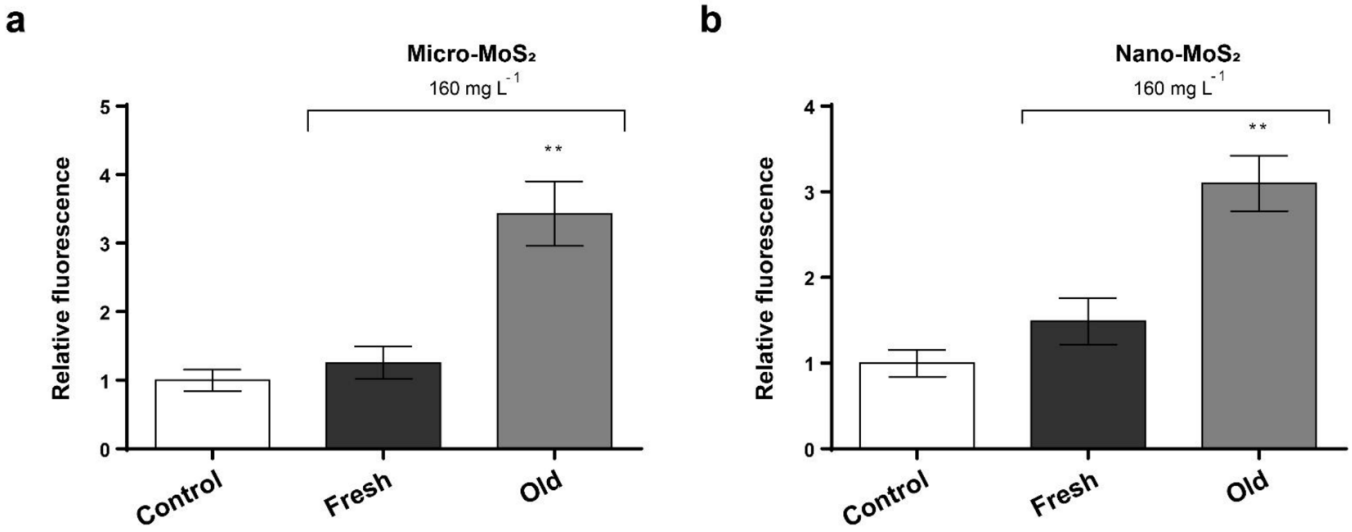

Figure 7. ROS production of A549 cells exposed to 160 mg l^{-1} of fresh and old micro-MoS_2 (a) and nano-MoS_2 (b) for 1 h. The reported values are expressed in arbitrary units and correspond to the averages of two biological replicates per culture condition. Data represent the mean of two replicates (±standard deviation, SD). Differences were established using a one-way ANOVA followed by Dunnett's post hoc test to compare every mean with the control and considered significant at $P \leq 0.05$; $^{**}P \leq 0.01$.

in figure 8, their impact on the viability of yeast cells was dependent on the product type, concentration and exposure time.

After a short exposure time (2 h), no significant viability changes were observed in the different conditions tested, except for that of yeast cells exposed to the high concentration of old nano-MoS_2, where an average decrease on CFUs of 20% was observed. However, a clear decrease on yeast viability was observed in exposures of 24 h, being more drastic when cells were exposed to the old suspensions of both nanoparticle types. The toxicity provoked by micro-MoS_2 and nano-MoS_2 was comparable. In the presence of 160 mg l^{-1}, the fresh nanoparticles suspensions induced a decrease on yeast viability of ∼40%, while the presence of 800 mg l^{-1} reduced the CFUs around 70%. In case of the old nanoparticles suspensions, 160 mg l^{-1} reduced the yeast cells viability 50% to 60%, while in the presence of the higher concentration only 1% of the exposed cells survived.

As previously mentioned, the higher toxicity levels induced by the old samples, this time in *S. cerevisiae* cells, suggest a possible mixture toxicity effect produced by the MoS_2 nanosheets transformation products. The fact that 160 mg l^{-1} of both fresh and old nanoparticles were able to reduce the viability of *S. cerevisiae* indicates that these products are more toxic for yeast cells than for the A549 cell line. Previous studies have demonstrated the antimicrobial properties of MoO_3 [45, 46], while the antifungal properties of SO_2 are well known [47], which could explain the higher toxicity observed. Yu

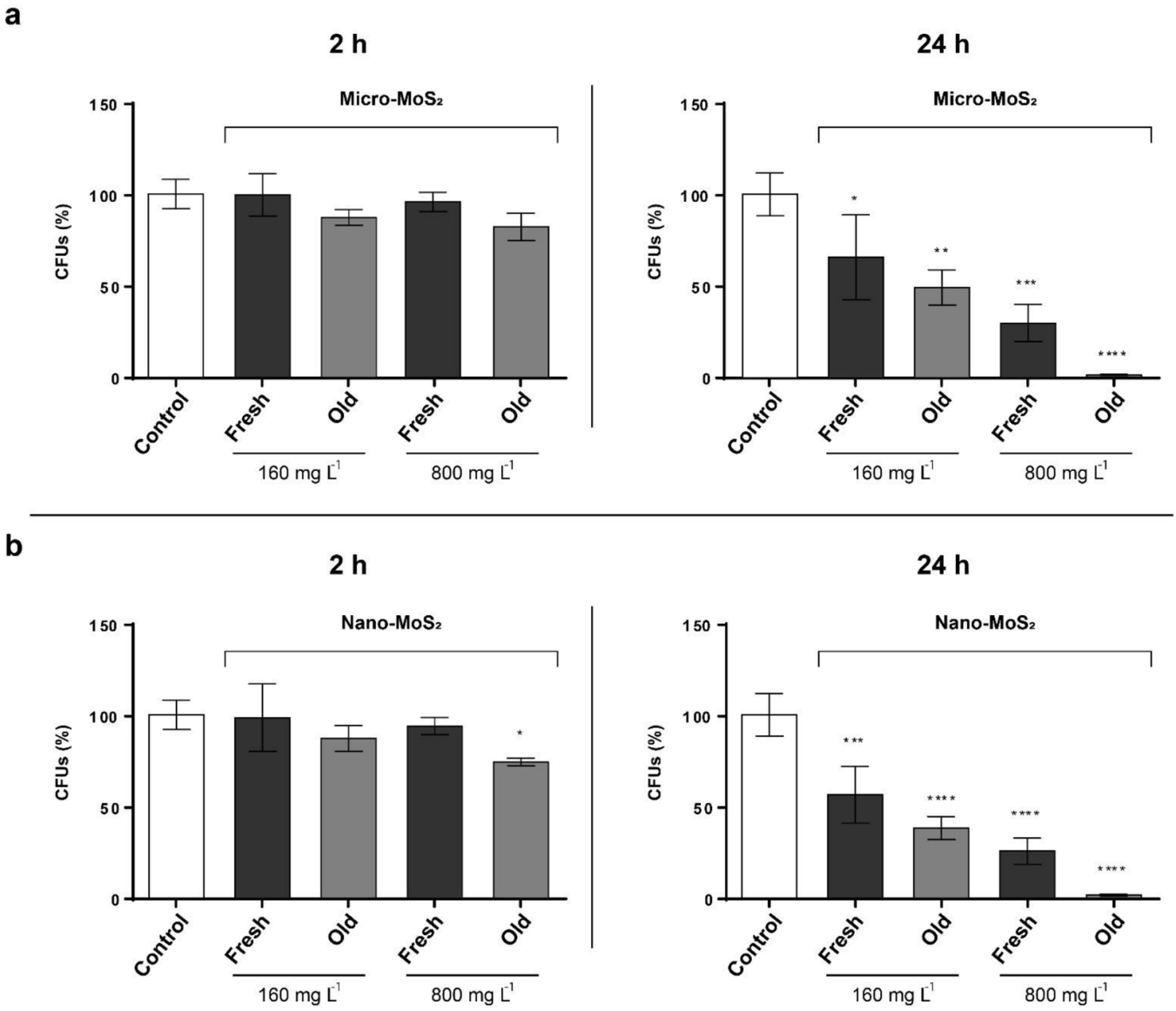

Figure 8. Colony forming units (CFUs) determination of *S. cerevisiae* cells exposed to 160 and 800 mg l^{-1} of fresh and old micro-MoS_2 (a) and nano-MoS_2 (b), for 2 and 24 h. The reported values are the averages of three biological replicates per culture condition. Differences were established using a one-way ANOVA followed by Dunnett's post hoc test to compare every mean with the control, and considered significant at $P \leq 0.05$, $^{*}P \leq 0.05$, $^{***}P \leq 0.001$, $^{****}P \leq 0.0001$.

et al investigated the exposure of yeast cells to bulk MoS_2, concluding that concentrations higher than 1 mg l^{-1} could produce a negative effect on the cell membrane integrity and inducing ROS accumulation, possibly due to the discrete crystal planes and surface defects of the material [19]. Many studies have demonstrated that fungal cells toxicity of nanomaterials, including MoS_2 and its transformation products, often involve oxidative stress and ROS [19, 46, 48–51]. Therefore, to find out whether the selected MoS_2 nanoparticles could also increase the intracellular ROS level in yeast cells, we exposed the BY4741 strain to 160 and 800 mg l^{-1} of the fresh and old samples for 2 h (see section 2). As shown in the figure 9, no significant differences in ROS levels were observed between the control condition and the conditions were yeast cells were exposed to 160 mg l^{-1} of the different nanomaterials suspensions. However, 800 mg l^{-1} of both types of fresh nanomaterials increased ROS significantly, while the same concentration of the old suspensions increased the oxidative stress levels at a minor, non-significant level. This result indicates that the fresh nanoparticles have a higher capacity to induce oxidative stress in yeast cells. Also, that the toxicity mechanisms induced by the old nanoparticles suspensions are not necessarily associated to the presence of ROS, at least at an early exposure stage. Nevertheless, ROS measurements on *S. cerevisiae* cells exposed to the old nanomaterials suspensions (160 mg l^{-1}) for 24 h showed that oxidative stress levels where three times higher in the test conditions than in the control condition, indicating that the transformation products of the MoS_2 nanosheets are also able to induce significant ROS levels in yeast cells.

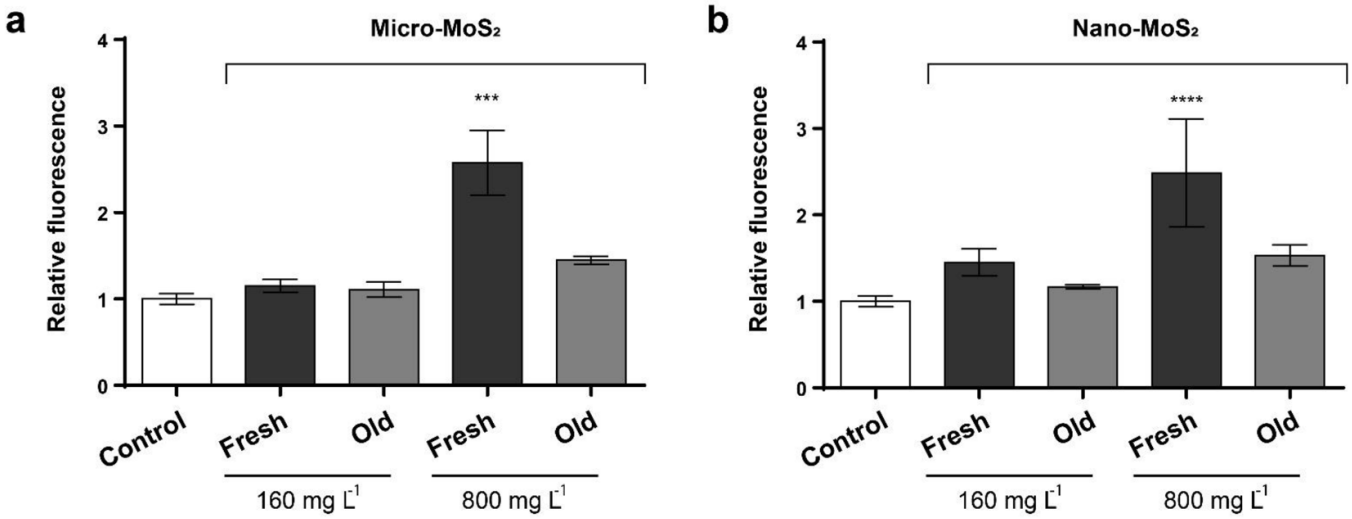

Figure 9. Oxidative stress (ROS) determination of *S. cerevisiae* cells exposed to 160 and 800 mg l^{-1} of fresh and old micro-MoS_2 (a) and nano-MoS_2 (b) during 2 h. The reported values are expressed in arbitrary units and correspond to the averages of two biological replicates per culture condition. Differences were established using a one-way ANOVA followed by Dunnett's post hoc test to compare every mean with the control, and considered significant at $P \leq 0.05$, $^{***}P \leq 0.001$, $^{****}P \leq 0.0001$.

The use of N-doped MoS_2 nanostructures and MoO_3 as antifungal agents have been recently explored [46, 51]. The results obtained in the present study also indicate that MoS_2 nanomaterials have antifungal properties, producing an enhanced effect once they are degraded and transformed in a mix of MoO_x, oxysulfide, and MoS_xO_y species. The use of chemicals as nanoparticles in fungicidal applications is a good alternative to the use of bulk forms, due to their higher dispersibility and larger surface to volume ratio, and to the use of ionic forms, thanks to their lower leachability.

4. Conclusion

The results obtained in the present study provide novel insights into the fate of MoS_2 nanoparticles in aqueous suspensions and their toxicological impact on different biological systems at distinct material life cycle stages. The morphological analysis of commercial micro-MoS_2 and nano-MoS_2 determined a lateral size in the nanoscale range for both products, while the analysis of their structure and chemical composition through Raman and XPS revealed high similarity between both pristine nanomaterials, but remarkable differences in the chemical composition of fresh and old water suspensions. Nano-MoS_2 nanoparticles stored as aqueous suspensions were degraded faster, but in both cases 10 months old suspensions were highly enriched in a mixture of defected MoS_x species, and oxysulfides MoS_xO_y. The differences in composition of fresh and old MoS_2 aqueous suspensions affected their toxicological impact, which was evaluated using human A549 cells and the yeast *S. cerevisiae*. Different toxicity levels for both model organisms were observed when using comparable exposure conditions. While the selected nanoparticles provoked a sublethal damage on the A549 cells though the increase of intracellular ROS levels, equal concentrations reduced the viability of yeast cells. Additionally, the old MoS_2 nanoparticles suspensions showed higher toxicity for both human and yeast cells than the fresh ones. The presented results highlight the relevance of analyzing the fate of nanomaterials at physicochemical and toxicological level to increase the understanding on their characteristics and their potential impact on biological systems along their life cycle.

Acknowledgments

We would like to thank Sonia Martel and Rocio Barros for their invaluable support.

Funding sources

This work was supported by the European Union's H2020 research and innovation programme under the Marie Skłodowska-Curie grant agreement Nº 721642.

Conflict of interest

The authors declare that they have no conflict of interests.

ORCID iDs

Kapil Bhorkar https://orcid.org/0000-0001-8062-8639
Labrini Sygellou https://orcid.org/0000-0001-8466-7029
Spyros N Yannopoulos https://orcid.org/0000-0001-6684-3172
Juan Antonio Tamayo-Ramos https://orcid.org/0000-0002-7071-002X

References

[1] Fojtů M, Teo W Z and Pumera M 2017 Environmental impact and potential health risks of 2D nanomaterials *Environ. Sci. Nano* **4** 1617–33

[2] Zhang H 2015 Ultrathin two-dimensional nanomaterials *ACS Nano* **9** 9451–69

[3] Liu T and Liu Z 2018 2D MoS_2 nanostructures for biomedical applications *Adv. Healthcare Mater.* **7** 1701158

[4] Ganatra R and Zhang Q 2014 Few-layer MoS_2 : a promising layered semiconductor *ACS Nano* **8** 4074–99

[5] Vazirisereshk M R, Martini A, Strubbe D A and Baykara M Z 2019 Solid lubrication with MoS_2: a review *Lubricants* **7**

[6] Jian J, Chang H and Xu T 2019 Structure and properties of single-layer MoS 2 for nano-photoelectric devices *Materials (Basel)* **12** 1–10

[7] Barua S, Dutta H S, Gogoi S, Devi R and Khan R 2017 Nanostructured MoS_2-based advanced biosensors: a review *ACS Appl. Nano Mater.* **1** 2–25

[8] Zeng G, Chen T, Huang L, Liu M, Jiang R, Wan Q, Dai Y, Wen Y, Zhang X and Wei Y 2018 Surface modification and drug delivery applications of MoS_2 nanosheets with polymers through the combination of mussel inspired chemistry and SET-LRP *J. Taiwan Inst. Chem. Eng.* **82** 205–13

[9] Yin F, Anderson T, Panwar N, Zhang K, Tjin S C, Ng B K, Yoon H S, Qu J and Yong K-T 2018 Functionalized MoS_2 nanosheets as multi-gene delivery vehicles for *in vivo* pancreatic cancer therapy *Nanotheranostics* **2** 371–86

[10] Wu S, Wang J, Jin L, Li Y and Wang Z 2018 Effects of polyacrylonitrile/MoS_2 composite nanofibers on the growth behavior of bone marrow mesenchymal stem cells *ACS Appl. Nano Mater.* **1** 337-343

[11] Yang X, Li J, Liang T, Ma C, Zhang Y, Chen H, Hanagata N, Su H and Xu M 2014 Antibacterial activity of two-dimensional MoS_2 sheets *Nanoscale* **6** 10126–33

[12] Chng E L K, Sofer Z and Pumera M 2014 MoS_2 exhibits stronger toxicity with increased exfoliation *Nanoscale* **6** 14412–8

[13] Appel J H, Li D O, Podlevsky J D, Debnath A, Green A A, Wang Q H and Chae J 2016 Low cytotoxicity and genotoxicity of two-dimensional MoS_2 and WS_2 *ACS Biomater. Sci. Eng.* **2** 361–7

[14] Moore C, Movia D, Smith R J, Hanlon D, Lebre F, Lavelle E C,, Byrne H J, Coleman J N, Volkov Y and McIntyre J 2017 Industrial grade 2D molybdenum disulphide (MoS_2): an *in vitro* exploration of the impact on cellular uptake, cytotoxicity, and inflammation *2D Mater.* **4** 025065

[15] Kaur J *et al* 2018 Biological interactions of biocompatible and water-dispersed MoS_2 nanosheets with bacteria and human cells *Sci. Rep.* **8** 16386

[16] Kenry and Lim C T 2017 Biocompatibility and nanotoxicity of layered two-dimensional nanomaterials *ChemNanoMat* **3** 5–16

[17] Alimohammadi F, Sharifian M, Attanayake N H, Thenuwara A C, Gogotsi Y, Anasori B and Strongin D R 2018 Antimicrobial properties of 2D MnO_2 and MoS_2 nanomaterials vertically aligned on graphene materials and Ti_3C_2 MXene *Langmuir* **34** 7192–200

[18] Yang Q, Zhang L, Ben A, Wu N, Yi Y, Jiang L, Huang H and Yu Y 2018 Effects of dispersible MoS_2 nanosheets and nano-silver coexistence on the metabolome of yeast *Chemosphere* **198** 216–25

[19] Yu Y *et al* 2017 Effect of bulk MoS_2 on the metabolic profile of yeast *J. Nanosci. Nanotechnol.* **18** 3901–7

[20] Wang Z, Von Dem Bussche A, Qiu Y, Valentin T M, Gion K, Kane A B and Hurt R H 2016 Chemical dissolution pathways of MoS_2 nanosheets in biological and environmental media *Environ. Sci. Technol.* **50** 7208–17

[21] Zhang X, Jia F, Yang B and Song S 2017 Oxidation of molybdenum disulfide sheet in water under *in situ* atomic force microscopy observation *J. Phys. Chem.* C **121** 9938–43

[22] Fröhlich E and Salar-Behzadi S 2014 Toxicological assessment of inhaled nanoparticles: role of *in vivo, ex vivo, in vitro*, and *in silico* studies *Int. J. Mol. Sci.* **15** 4795–822

[23] Braconi D, Bernardini G and Santucci A 2016 *Saccharomyces cerevisiae* as a model in ecotoxicological studies: a post-genomics perspective *J. Proteomics* **137** 19–34

[24] Hu K H, Hu X G, Wang J, Xu Y F and Han C L 2012 Tribological properties of MoS_2 with different morphologies in high-density polyethylene *Tribol. Lett.* **47** 79–90

[25] Lee C, Yan H, Brus L E, Heinz T F, Hone J and Ryu S 2010 Anomalous lattice vibrations of single- and few-layer MoS_2 *ACS Nano* **4** 2695–700

[26] Kumari L, Ma Y R, Tsai C C, Lin Y W, Wu S Y, Cheng K W and Liou Y 2007 X-ray diffraction and Raman scattering studies on large-area array and nanobranched structure of 1D MoO_2 nanorods *Nanotechnology* **18** 115717

[27] Ahmed B, Shahid M, Nagaraju D H, Anjum D H, Hedhili M N and Alshareef H N 2015 Surface passivation of MoO_3 nanorods by atomic layer deposition toward high rate durable Li ion battery anodes *ACS Appl. Mater. Interfaces* **7** 13154–63

[28] Kondekar N P, Boebinger M G, Woods E V and McDowell M T 2017 *In situ* XPS investigation of transformations at crystallographically oriented MoS_2 interfaces *ACS Appl. Mater. Interfaces* **9** 32394–404

[29] Liang X, Hart C, Pang Q, Garsuch A, Weiss T and Nazar L F 2015 A highly efficient polysulfide mediator for lithium-sulfur batteries *Nat. Commun.* **6** 1–8

[30] Marletta G and Iacona F 1996 Chemical selectivity and energy transfer mechanisms in the radiation-induced modification of polyethersulphone *Nucl. Instrum. Methods Phys. Res.* B **116** 246–52

[31] Lanone S, Rogerieux F, Geys J, Dupont A, Maillot-Marechal E, Boczkowski J, Lacroix G and Hoet P 2009 Comparative toxicity of 24 manufactured nanoparticles in human alveolar epithelial and macrophage cell lines *Part. Fibre Toxicol.* **6** 1–12

[32] Costa C *et al* 2016 In vitro cytotoxicity of superparamagnetic iron oxide nanoparticles on neuronal and glial cells. Evaluation of nanoparticle interference with viability tests *J. Appl. Toxicol.* **36** 361–72

[33] Repetto G, Del Peso A and Zurita J L 2008 Neutral red uptake assay for the estimation of cell viability/cytotoxicity *Nat. Protocol* **3** 1125–31

[34] Wang X *et al* 2015 Differences in the toxicological potential of 2D versus aggregated molybdenum disulfide in the lung *Small* **11** 5079–87

[35] Mei L, Zhang X, Yin W, Dong X, Guo Z, Fu W, Su C, Gu Z and Zhao Y 2019 Translocation, biotransformation-related degradation, and toxicity assessment of polyvinylpyrrolidone-modified 2H-phase nano-MoS_2 *Nanoscale* **11** 4767–80

[36] Teo W Z, Chng E L K, Sofer Z and Pumera M 2014 Cytotoxicity of exfoliated transition-metal dichalcogenides (MoS_2, WS_2, and WSe_2) is lower than that of graphene and its analogues *Chem. Eur. J.* **20** 9627–32

[37] Pujalté I, Passagne I, Brouillaud B, Tréguer M, Durand E, Ohayon-Courtès C and L'Azou B 2011 Cytotoxicity and oxidative stress induced by different metallic nanoparticles on human kidney cells *Part. Fibre Toxicol.* **8** 10

[38] Khanna P, Ong C, Bay B and Baeg G 2015 Nanotoxicity: an interplay of oxidative stress, inflammation and cell death *Nanomaterials* **5** 1163–80
[39] Aranda A, Sequedo L, Tolosa L, Quintas G, Burello E, Castell J V and Gombau L 2013 Dichloro-dihydro-fluorescein diacetate (DCFH-DA) assay: A quantitative method for oxidative stress assessment of nanoparticle-treated cells *Toxicol. Vitro* **27** 954–63
[40] Yu Y, Wu N, Yi Y, Li Y, Zhang L, Yang Q, Miao W, Ding X, Jiang L and Huang H 2017 Dispersible MoS_2 nanosheets activated TGF-β/Smad pathway and perturbed the metabolome of human dermal fibroblasts *ACS Biomater. Sci. Eng.* **3** 3261–72
[41] Liu S, Shen Z, Wu B, Yu Y, Hou H, Zhang X X and Ren H Q 2017 Cytotoxicity and efflux pump inhibition induced by molybdenum disulfide and boron nitride nanomaterials with sheetlike structure *Environ. Sci. Technol.* **51** 10834–42
[42] National Toxicology Program 1997 NTP toxicology and carcinogenesis studies of nitromethane (CAS No. 75-52-5) in F344/N rats and B6C3F1 mice (inhalation studies) *Natl. Toxicol. Progr. Tech. Rep. Ser.* **461** 1–289
[43] Anh Tran T, Krishnamoorthy K, Song Y W, Cho S K and Kim S J 2014 Toxicity of nano molybdenum trioxide toward invasive breast cancer cells *ACS Appl. Mater. Interfaces* **6** 2980–6
[44] Kwolek-Mirek M and Zadrag-Tecza R 2014 Comparison of methods used for assessing the viability and vitality of yeast cells *FEMS Yeast Res.* **14** 1068–79
[45] Shafaei S, Van Opdenbosch D, Fey T, Koch M, Kraus T, Guggenbichler J P and Zollfrank C 2016 Enhancement of the antimicrobial properties of orthorhombic molybdenum trioxide by thermal induced fracturing of the hydrates *Mater. Sci. Eng. C* **58** 1064–70
[46] Chaves-Lopez C, Nguyen H N, Oliveira R C, Nadres E T, Paparella A and Rodrigues D F 2018 A morphological, enzymatic and metabolic approach to elucidate apoptotic-like cell death in fungi exposed to h- and α-molybdenum trioxide nanoparticles *Nanoscale* **10** 20702–16
[47] King A D, Ponting J D, Sanshuck D W, Jackson R and Mihara K 1981 Factors affecting death of yeast by sulfur dioxide *J. Food Prot.* **44** 92–97
[48] Sousa C A, Soares H M V M and Soares E V 2018 Nickel oxide (NiO) nanoparticles induce loss of cell viability in yeast mediated by oxidative stress *Chem. Res. Toxicol.* **31** 658–65
[49] Domi B, Rumbo C, García-Tojal J, Elena Sima L, Negroiu G and Tamayo-Ramos J A 2019 Interaction analysis of commercial graphene oxide nanoparticles with unicellular systems and biomolecules *Int. J. Mol. Sci.* **21** 205
[50] Suarez-Diez M, Porras S, Laguna-Teno F, Schaap P J and Tamayo-Ramos J A 2020 Toxicological response of the model fungus *Saccharomyces cerevisiae* to different concentrations of commercial graphene nanoplatelets *Sci. Rep.* **10** 1–12
[51] Basu P *et al* 2019 Defect-engineered MoS_2 nanostructures for reactive oxygen species generation in the dark: antipollutant and antifungal performances *ACS Appl. Mater. Interfaces* **11** 48179–91